V European Conference on Computational Fluid Dynamics
ECCOMAS CFD 2010
J. C. F. Pereira and A. Sequeira (Eds)
Lisbon, Portugal,14-17 June 2010

LARGE EDDY SIMULATION IN GENERALIZED CURVILINEAR COORDINATES AND ITS APPLICATION TO AN AXISYMMETRIC DUMP COMBUSTOR(ECCOMAS CFD 2010)

Balram Panjwani*, Ivar S. Ertesvåg *, Andrea Gruber† & Kjell Erik Rian‡

*Department of Energy and Process Engineering,
Norwegian University of Science and Technology,Trondheim
e-mail: balram.panjwani@ntnu.no
†SINTEF Energy Research, Trondheim
‡ Computational Industry Technologies (ComputIT), N-7462 Trondheim, Norway

Key words: LES, curvilinear coordinates, conventional and alternate filtering, dump combustor, Backward Facing Step

Abstract. *Large Eddy simulation (LES) methodology in curvilinear coordinates is presented. In the current LES formulation filtering and coordinate transformation are decoupled and filtering is performed prior to the transformation as against the "alternate approach" proposed by Jordan , where filtering is done after the transformation. The relative advantages and disadvantages of this approach are discussed. Filtering in physical space introduces a commutation error between filtering and differentiation due to non-uniform meshes. This error and its consequence on overall accuracy is discussed. The commutation filter defined in generalized coordinates is presented. In order to save computational time for simple geometries the orthogonal and non-orthogonal terms are treated separately in the present simulation. The approach is validated by studying the flow over a backward facing step (BFS) and an axis-symmetric dump combustor (ACDC). The LES simulation of the BFS is carried out for a Reynolds number of 5100 based on the inlet free-stream velocity and step height h. The results are validated against DNS data. The mean longitudinal, vertical velocity profile and the turbulence intensities compare satisfactory with the DNS data at the normalized coordinates. The reattachment length in the longitudinal direction varies from 7.1h to 7.3h as compared to the DNS value of 6.28h. In addition, a simulation of the ACDC is carried out for a Reynolds number of 11700 based on the guiding pipe diameter and the bulk velocity. In order to save computational time, only a 90 degree segment of the geometry is studied. The results are validated against an experimental data base and the consequences of the calculation approach on the overall accuracy are assessed. The reattachment length was well predicted and the mean longitudinal, vertical velocity profile and the turbulence intensities compare satisfactory with the experiments. It is also observed that the influence of the SGS model is less crucial than the discretization and the grid resolution. The overall accuracy depends on the discretization scheme, the grid resolution, inflow and other boundary conditions.*

1 Introduction

Modeling of fluid flow by numerical simulation includes Reynolds Averaged Navier Stokes (RANS), Large Eddy Simulation (LES) and Direct Numerical Simulation (DNS). In RANS, ensemble or time averaged Navier Stokes(N-S) equations are solved and turbulence is modeled using an appropriate turbulence model, whereas DNS solves N-S equation on the grid scales without any turbulence model but it is computationally demanding. LES, which resolves a major part of turbulent kinetic energy is a promising tool for understanding the physics of unsteady turbulent flow at comparatively reduced costs. In LES, the large geometrically dependent energy-carrying eddies are resolved on grid scales(GS), whereas effects of the smaller, more universal scales are modeled using a sub-grid scale (SGS) model. A high fidelity LES should resolve length scales from the largest to the inertial scale on the grid scales. A wide range of subgrid models have been studied and successfully applied to LES.[1–3] Over the decades LES has been applied successfully to the simple as well as complex geometries. Grigoriadis et al.[4] presented an LES method to treat complex geometrical configurations using the domain decomposition approach and the immersed boundary method. Mahesh et al.[5] developed an LES method for complex geometries discretized with unstructured hybrid grid. LES methodology in curvilinear coordinates has been used for many complex geometries[6–8]

In present study a LES methodology is presented in body fitted curvilinear coordinates. LES formulation in curvilinear coordinates poses a basic problem, whether filtering has to be performed prior or after the transformation. This problem has been studied by Jordan[6] and he defined the conventional and alternate approaches. In the conventional approach, filtering is performed before transformation and in the alternate approach filtering is performed after the transformation. Jordan favored the alternate approach due to ill defined filter and unfiltered representation of metrics coefficients in physical space. But he also mentioned that there was no difference in the spectral energies of the turbulent fluctuation by filtering in either physical or computational space. In the present methodology filtering before the transformation was preferred and transformation was considered as a mathematical operator to represent the governing equations in curvilinear coordinates. In the present simulation the Leonard term was defined in the physical space and then coordinate transformation was performed. Finally, Jordan[6] did not mention any strong reasons for not using the conventional approach except the filter definition in physical space and representation of metric coefficients. The present paper discuss more on merits and demerits of alternate and conventional approaches.

The accuracy of a numerical simulation with LES depends on the discretization schemes, the grid resolutions and the subgrid-scale (SGS) models. In LES, numerical diffusion caused by the truncation error of a low-order finite-volume discretization scheme (FVDS) can be of the same order of magnitude as the subgrid turbulence viscosity.[9,10] Since the numerical diffusion does not represent the turbulence cascade mechanism and subsequent turbulent diffusion by smaller eddies. Hence, proper SGS modeling is essential in order to model the role of smaller eddies.

The present LES methodology, which uses the conventional approach, was validated by studying the unsteady turbulent flow, over a backward facing step (BFS) and in an axisymmet-

ric confined dump combustor (ACDC). Although the BFS flow is geometrically simple but it involves very complex phenomena. At the corner of the step, the separated upstream boundary layer forms a free-shear layer. The free shear-layer attaches downstream at the reattachment point X_r and oscillate in the longitudinal direction. The fluid, upstream to the reattachment point is subjected to an adverse pressure gradient and forms a separation bubble. Non-reacting flows over BFS has been studied extensively both experimentally and numerically, and it is one of the benchmark test case in turbulence modeling.[11–15] In the present paper unsteady characteristics of the BFS and its dynamics with numerical scheme, subgrid model and grid resolution is studied.

Efficient combustion requires proper mixing between the fuel and oxidizer for non-premixed flames and between burnt and unburnt mixture for premixed flames. The mixing phenomena and other combustion processes inside the dump combustor is influenced by vortices's that are formed in the shear layer. Several experimental and numerical studies have been carried out for a dump combustor with and without swirl to understand the unsteadiness, vortex breakdown mechanism ,etc., for reacting and non reacting flows.[16–18] Lucca and Negro[19] have reviewed the numerical, experimental and theoretical work on vortex breakdown. In the present work flow inside the dumb combustor was studied without swirl for which previous experimental and numerical data sets were available[17,20]

Axisymmetric geometries are quite common in practical and industrial problems and most of the simulations are performed over a pie segment to save computational time. This is true for time averaged RANS simulation where the axis boundary condition is modeled with proper boundary condition on turbulent kinetic energy and dissipation. In case of LES where instantaneous evolution of flow quantities take place. Then the axis boundary condition is not appropriate especially for confined jet and swirl flow where momentum, mass etc exchange take place across the axis. This issue has been studied by Schlüter[21] and he observed a substantial differences in velocities and fluctuations especially close to the axis. The similar behavior have been observed in present study also.

2 Governing equations and filtering

Three dimensional time dependent Navier-Stokes equations in generalized curvilinear coordinate in strong conservation law form[22] were used in the present work. The N-S equations were filtered using an implicit low pass box filter in physical space.[8,10]
The filtered continuity equation for flow with constant density is expressed as

$$\frac{\partial J\widetilde{U^k}}{\partial \xi^k} = 0 \tag{1}$$

The filtered momentum equation

$$\frac{\partial J\widetilde{\rho}\,\widetilde{u}_i}{\partial t} + \frac{\partial \widetilde{\rho} J\widetilde{U^k}\widetilde{u}_i}{\partial \xi^k} = -\frac{\partial J\xi_i^k \widetilde{p}}{\partial \xi^k} + \frac{\partial}{\partial \xi^k}\left(\mu J\xi_j^k\left(\xi_j^l\frac{\partial \widetilde{u}_i}{\partial \xi^l} + \xi_i^l\frac{\partial \widetilde{u}_j}{\partial \xi^l}\right)\right) - \frac{\partial J\widetilde{\rho}\xi_j^k\tau_{ij}}{\partial \xi^k} \tag{2}$$

Where, summation rule applies to all indices except indices i, u_i denotes the Cartesian component of the velocity field, ρ is the density, p is the static pressure, μ is the molecular viscosity, ξ^k is the coordinates direction in the transformed space, $\xi^k_j = \partial\xi^k/\partial x_j$, J is the Jacobian of the coordinates transformation, $U^k = \xi^k_j u_j$ are the contravariant velocities components and $\widetilde{\phi}$ represents the filtered quantities of a variable ϕ. Further, the subgrid stress τ_{ij} can be expressed as

$$\tau_{ij} = L_{ij} + C_{ij} + R_{ij} \tag{3}$$

$$\tau_{ij} = \widetilde{u_i u_j} - \widetilde{u}_i \widetilde{u}_j \tag{4}$$

Term $L_{ij} = \widetilde{\widetilde{u}_i \widetilde{u}_j} - \widetilde{u}_i \widetilde{u}_j$ is called the Leonard term and represents the interactions among the larger scales. $C_{ij} = \widetilde{\widetilde{u}_i u'_j} + \widetilde{\widetilde{u}_j u'_i}$ is called the cross-stress term and represents the interaction between the larger eddies and smaller eddies and $R_{ij} = \widetilde{u'_i u'_j}$ is called the Reynolds subgrid tensor. The subgrid stress τ_{ij} is calculated using eddy viscosity approach.

$$\tau_{ij} - \frac{1}{3}\delta_{ij}\tau_{kk} = -2\nu_t \widetilde{S}_{ij} \tag{5}$$

where $\widetilde{S}_{ij} = \left(\xi^l_j \frac{\partial \widetilde{u}_i}{\partial \xi^l} + \xi^l_i \frac{\partial \widetilde{u}_j}{\partial \xi^l}\right)$ is the filtered strain rate tensor. Hence,

$$\tau_{ij} = \left(-\nu_t \left(\xi^l_j \frac{\partial \widetilde{u}_i}{\partial \xi^l} + \xi^l_i \frac{\partial \widetilde{u}_j}{\partial \xi^l}\right) + \frac{2}{3}\delta_{ij}\widetilde{k}\right) \tag{6}$$

where, ν_t, is the eddy viscosity. In the present study the Smagorinsky model is employed to compute the eddy viscosity.

$$\nu_t = (C_s \Delta)^2 \, |\widetilde{S}| \tag{7}$$

$$|\widetilde{S}| = \sqrt{2\widetilde{S}_{ij}\widetilde{S}_{ij}} \tag{8}$$

Where, C_s is a constant and can be estimated dynamically, and $\Delta = \left(J\delta\xi^l\delta\xi^2\delta\xi^3\right)^{1/3}$ is the filter width.

3 Conventional vs Alternate Approach

In the present study, the conventional approach was preferred rather than the alternate approach. Jordan[6] mentioned a difficulty in calculating the Leonard term due to ill defined filter in physical space. But in actual practice the Leonard term represents the interaction among larger eddies and can be evaluated in the physical space with an appropriate filter kernel developed in physical space. Similarly other terms, such as the cross stress and Reynolds stress terms also need to be evaluated in the physical space. In the alternate approach, all these terms were formulated based on the contravariant velocity components, where interaction among contravariant components is still not clear. Another issue with the Leonard term in computational space is its inherent metric coefficients, which has to be evaluated with higher order schemes.

Jordan[6] also pointed out with the conventional approach, the metric coefficients need to evaluated exactly. But for practical cases this is an option and not a constraint. In the conventional approach the analytic treatment of the metric coefficients and the Jacobian for tightly controlled grids give improvement in the solution with fewer grids.[23] But in complex geometry this condition is difficult to meet and then the numerical treatment of the metric coefficients and Jacobian is the most preferred choice.[23] Finally, Jordan[6] carried out a priori test with a DNS data set of the wake of a circular cylinder at a Reynolds number of 3400 using a filter developed in physical as well as in computational space, but he did not observe any difference in the respective damped spectral energies except the cost of the filter. In LES the cost of explicit filtering is hardly 5-6% of total cost. Finally there were no strong reasons mentioned for avoiding the conventional approach except for the numerical implementation. In fact the alternate approach posed some difficulty while evaluating the dynamic model constant.

3.1 Practical Difficulty with Alternate Approach

LES in non-orthogonal coordinate have been used many times without reference to the alternate or conventional approaches. Mostly LES methodologies in curvilinear coordinates are based on conventional approach. Moin and Kim[10] developed an unsteady high-order LES solver using a localized dynamic model (LKDM). In their study, a methodology was developed in physical space and then transformation was used to represent the governing equation in computational space.

Jordan and Ragab[24] formulated a dynamic model in the alternated approach by contracting the Germano identity $\left(\Gamma_i^k = \Upsilon_i^k - \widetilde{\sigma}_i^k\right)$ with $M_i^k = J\xi_j^k M_{ij}$. They obtained a dynamic model constant as $C_{alter} = -\frac{1}{2}\frac{<\Gamma_i^k M_i^k>}{<M_n^m M_n^m>}$. Where σ_i^k are the subgrid stress tensor in computational space, Γ_i^k are the contravariant resolved turbulent stresses and Υ_i^k are the contravariant resolved subgrid stresses. Armenio and Piomelli,[7] who developed a Lagrangian dynamic mixed model in generalized coordinates using the alternate approach, brought out an issue of constriction of the Germano identity. According to them, computed subgrid viscosity using C_{alter} was not rotationally invariant. The remedy to this problem was to transform the Germano identity first in the physical space and then carry out the contraction. With this approach the dynamic model constant was given by $C_s = -\frac{1}{2}\frac{<\Gamma_i^k M_i^q G_{kq}>}{<M_n^m M_n^l G_{ml}>}$. Where $M_i^m M_i^l G_{ml} = M_{ij} M_{ij}$.[7] This approach is similar to developing a dynamic constant in physical space.

In implementation of Lagrangian model,[7] a two step procedure was used, where first all turbulent quantities (velocities etc) were transformed into a contravariant form. These contravariant quantities were filtered using three point top hat filter and then transferred back in physical space. Pre and post transformation of flow quantities can introduce substantial damping due to low order approximation of metric coefficients[6] . Finally, implementing any new subgrid models with alternate approach require the modification of model, like Lagrangian dynamic mixed model, and subsequent testing of the models

3.2 Filter for Body fitted Curvilinear Geometries

For evaluating the dynamic constant explicit filtering is required. Ghosal and Moin[25] studied the commutation problem of differentiation and filtering with non uniform grid, according to them when any convolution filter is applied to the N-S equations under inhomogeneous flows and nonuniform grid then filtering and differentiation does not commute. $\widetilde{\frac{\partial \phi}{\partial x}} - \frac{\partial \widetilde{\phi}}{\partial x} \neq 0$. But practical flows are inhomogeneous and non-uniform grid is essential and filter has to be developed which can commute up to any order of filter width. Van Der Ven[26] constructed a filter for non-uniform grids which can commutes to any given order of the filter width. But this filter does not address problems of the boundary terms which arises in case of inhomogeneous flows. Vasilyev[27] presented a commutative filter for turbulent inhomogeneous flows and corresponding discrete filter in complex geometries upto any desired order of accuracy. The filter was developed in computational space using a mapping function. This approach differs from alternate approach, where N-S equations were filtered in computational space rather than the flow variables. Marsden et al.[28] extended the model developed by Vasilyev[27] for unstructured grid in physical space, which does not require any transformation.

Geurts et al.[29] studied the commutator errors and they mentioned that using a higher order filter can reduce the magnitude of the commutator error but also, flux due to turbulent stress is affected simultaneously in a same order of magnitude. They also mentioned that the commutation error can be controlled by selecting an appropriate filter width and filter skewness. But in complex geometry where filter width and skewness vary suddenly then explicit computation of the commutation error is essential.

Bahramian[30] proposed a volume based discrete filter that can be used for both structured and unstructured grids, but in their model the filtering operation commutes to one order less than the order of numerical scheme.

In non-orthogonal geometries, implementation of filter can be done in two ways. In first approach developed by Vasilyev,[27] primitive variables are transformed in contravariant form and then these contravariant quantities are filtered in computational space using a discrete filter developed by Vasilyev.[27] In second approach developed by Marsden,[28] primitive variables are filtered in physical space which requires calculation of a filter moments in complex geometry. The advantage with Marsden[28] approach is that it can be used for both structured and unstructured grid. The one dimensional filter proposed by Marsden[28]

$$\widetilde{f}\left(x\right) = f\left(x\right) + \sum_{l=n}^{l=\infty} \frac{\left(-1\right)^{l}}{l!} \triangle_{x}^{l} M^{l} \frac{\partial^{l} f}{\partial x} \tag{9}$$

Where $f\left(x\right)$ is a variable being filtered, G is the kernel of filter, $\triangle_x$ is the filter width and a & b are the domain boundaries. The filter moment M^l is defined as

$$M^{l} = \int_{(x-b)/\triangle_x}^{(x-a)/\triangle_x} \eta^{l} G\left(\eta, x\right) d\eta \tag{10}$$

Where $\eta = \left(x - y\right) / \triangle_x$ is the change of variable and y is associated with location dependent filter function $G\left(\frac{x-y}{\triangle_x}, x\right)$. The present finite volume schemes is second order accurate the

commutation error (which is also second order accurate) does not reduce the overall accuracy. Marsden[28] proposed a polynomial expression for filter moments $M^l = \sum_{k=0}^{k=\infty} W_k (x_k - x_0)^l$, which satisfy all the filter properties proposed by Vasilyev.[27] For second order accurate scheme, the filter moments $M^1 = 0$ and $M^2 \neq 0$ need to be evaluated. For one dimensional filter the second order filter moment is $M^2 = \frac{1}{(x_{i+1}+x_{i-1})^2} \left((x_i - x_{i-1})^2 + (x_{i+1} - x_i)^2 \right)$, where x_k and x_i are longitudinal positions of the grid and x_0 represent the longitudinal position where filter is being computed.

$$\widetilde{f}(x) = f(x) + \frac{M^2}{2} \frac{\partial}{\partial x} \left(\triangle_x^2 \frac{\partial f}{\partial x} \right) \tag{11}$$

In the present study three one dimensional filters, one in each direction, are employed. For uniform regular grid $M^2 = 1/2$, the filtered operator becomes a top hat filter $\widetilde{f_i} = f_i + \frac{1}{4}(f_{i+1} - 2f_i + f_{i-1})$.

4 The Dynamic Procedure in Conventional Approach

In the dynamic procedure[31] a second test filter gives a filtered sub grid stress (SGS) tensor T_{ij} similar to the original SGS σ_{ij} when applied to the filtered momentum equation in the physical space. The Germano identity in physical space is $L_{ij} = T_{ij} - \widetilde{\sigma}_{ij}$. Contracting the Germano identity with M_{ij} produces a dynamic constant in physical space

$$C_s = \frac{1}{2} \frac{L_{ij} M_{ij}}{M_{kl} M_{kl}} \tag{12}$$

where tensor $M_{kl} = \widetilde{\Delta}^2 \widehat{|\widetilde{S}|\widetilde{S}_{kl}} - \widehat{\widetilde{\Delta}^2} \widehat{|\widetilde{S}|} \widehat{\widetilde{S}}_{kl}$ and $L_{ij} = \widehat{\widetilde{u}_i \widetilde{u}_j} - \widehat{\widetilde{u}}_i \widehat{\widetilde{u}}_j$ and $\widehat{\widetilde{f}}(x)$ represent the double filtering of a variable $f(x)$. The stress tensor L_{ij} and M_{kl} are evaluated in physical space using the filter as expressed in Equ.(11). The constant C_s varies instantaneously with space and time and produces too much positive and too high negative subgrid viscosity, which destabilized the solution. To avoid the stability problem, in the present simulation averaging of the numerator and denominator in circumferential direction for ACDC and spanwise direction for BFS along with clipping is carried out.

5 Numerical Algorithm

The filtered NS Equ.(1) and Equ.(2) along with the subgrid stress Equ.(6) are solved using finite volume technique on a non-staggered grid. In the non-staggered grid all the variables (pressure, velocities components and scalars) are stored at the cell center. For calculating convective fluxes, flow variables at cell faces are required. This is achieved by a discretization technique such as Quadratic Upwind Differencing Scheme (QUICK) or the fourth order central scheme (CDS-4). The viscous fluxes are approximated by central differences scheme of second-order accurate. Rhie and Chow[32] moment interpolation (MI) scheme is used, to avoid the unphysical oscillations i.e. checker-board pressure on the non-staggered grid. In incompressible flow, density is not linked with pressure and for pressure-velocity coupling projection method[33] is used here. A three step (predictor-corrector-corrector) procedure is used here to

solve the filtered continuity and momentum equations. In the predictor step the momentum equations are solved to obtain intermediate velocities field with old pressure values. This intermediate velocities field do not satisfy the continuity equation. In the first corrector step the pressure correction $p^{'}$ is calculated by solving the pressure correction $p^{'}$ Poisson equation[3] Equ. (13) with the intermediate filtered velocities $\widetilde{u}_i^*$ field from the predictor step.

$$\frac{\partial}{\partial x_i}\left(\frac{\partial p^{'}}{\partial x_i}\right) = \frac{1}{\triangle t}\left(\frac{\partial \rho \widetilde{u}_i^*}{\partial x_i}\right) \tag{13}$$

Here $\triangle t$ is the time step. In the second corrector step, velocities and old pressure are corrected with computed pressure correction field from the first corrector step. The three-steps procedure is repeated until convergence. The governing momentum equations are integrated with an explicit five stage fourth-order Runge-Kutta method by Carpenter et al.[34] The orthogonal and non orthogonal terms are treated separately to save the computational time for simple geometries.

6 Problem Description

LES methodology was applied over the backward facing step (shown in Fig.1) and in the axisymmetric confined dump combustor (ACDC) (shown in Fig.2). BFS was chosen for its apparent geometrical simplicity, but it involves relatively complex flow phenomena. This geometry is well suited to study the turbulence behavior under separation, recirculation and reattachment,[35] which is of highly importance for many practical and engineering applications. Furthermore a well established amount of numerical and experimental literature are available[13–15, 36] for this case. The axisymmetric confined dump combustor (ACDC) was chosen due to complexity of geometry and flow. The experimental and numerical results show that the turbulence in the dump combustor is highly unsteady and anisotropic behind the sudden expansion.[16–18]

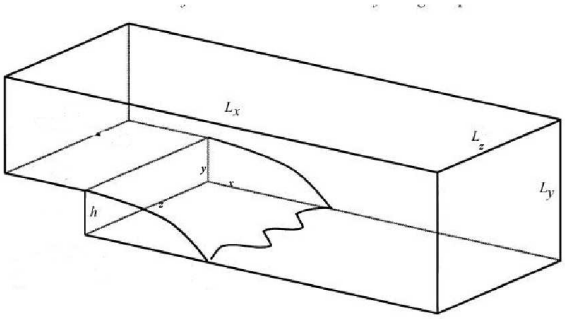

Figure 1: Geometrical Configuration of BFS

Figure 2: Geometrical Configuration of ACDC

6.1 Computational Domain

Figure 1 shows a computational domain used for BFS, where x, y and z represent the longitudinal, vertical and spanwise directions, respectively. The longitudinal length L_x of configuration was $20.5h$ and channel length ahead of the step was $2.5h$. The dimensions in the vertical L_y and

spanwise L_z directions were $6h$ and $4h$ respectively. The Reynolds number($Re_h = \rho U_0 h/\mu$) based on the step height and free stream velocity was 5100, which was same as the DNS of Le et al.[14] The computational domain was discretized using a grid $(148 \times 72 \times 20)$ in longitudinal, vertical and spanwise directions. The grid was refined in the strong shear flow regions, i.e. close to the walls and in recirculation region. The time step in the current simulation was fixed at $\Delta_t = 0.05h/U_0$. The total simulation time was $500h/U_0$. A no-stress wall $v = 0, \frac{\partial u}{\partial y} = 0, \frac{\partial w}{\partial y} = 0$ was applied at the upper boundary. No-slip boundary conditions was used at all walls. Where u, v and w are the velocity components in longitudinal, vertical and spanwise direction. A free-slip was imposed such that $w = 0, \frac{\partial u}{\partial z} = 0, \frac{\partial v}{\partial z} = 0$ on the spanwise boundaries. A mean turbulent profile by Spalart[37] at Re_θ = 670 supreimposed with a white noise was applied at inlet, where θ is a momentum thickness. The vertical and spanwise components of the mean velocity were set to zero. At outlet velocities gradient $\frac{\partial u_i}{\partial x_i} = 0$ were taken equal to zero.

Figure 2 shows the computational domain used for ACDC which is similar to the geometry studied by Wang et al.[17,20] The Reynolds number $(Re_B = \rho U_B d/\mu)$ for this configuration was 11700 based on the guiding pipe diameter d and the bulk velocity U_B. The diameters of the guiding pipe d, main pipe D and constriction pipe d were 25.3mm, 49.1 mm and 25.3mm respectively. The height $H = (D - d)$ of the sudden expansion (step) was 23.8mm. The length of guiding pipe, main pipe and constriction pipe were 2.1H, 17.44H and 2.1H respectively. In order to save computational time a quarter of cylinder (pie segment) was studied. A grid of $(154 \times 104 \times 20)$ was used in axial, radial and circumferential direction. At the inlet, longitudinal velocity profile from experiments[20] perturbed with white noise was used and radial and tangential component were set equal to zero. At outlet convective boundary condition $\frac{\partial u_i}{\partial t} + U_C \frac{\partial u_i}{\partial x_i} = 0$ was used. Where U_C was the convective velocity, which was assumed $U_C = U_B$. On the annular surface no slip wall boundary condition was used. The cyclic boundary condition was used on the circumferential direction. Time step in the current simulation was fixed at $\Delta_t = 4 \cdot 10^{-5}$. Total simulation time was 2s about 50000 time steps. Table 1 presents the different configurations studied for the LES over BFS and ACDC. For the BFS,

Table 1: LES Test Cases for Flow Over BFS and ACDC

Runs	Scheme	SGS model	Grid	Case Description
Run-1	QUICK	Dynamic (DM)	$(154 \times 88 \times 20)$	ACDC
Run-2	QUICK	Dynamic (DM)	$(154 \times 104 \times 20)$	ACDC
Run-3	CDS-4	Dynamic (DM)	$(154 \times 104 \times 20)$	ACDC
Run-4	QUICK	Dynamic (DM)	$(148 \times 72 \times 20)$	BFS
Run-5	CDS-4	Dynamic (DM)	$(148 \times 72 \times 20)$	BFS

the mean longitudinal velocity profiles and turbulent intensity non dimensionalized with inflow free stream velocity U_0 were computed and compared with DNS data set of Le et al.[14] For ACDC, mean longitudinal, radial velocity profiles and turbulent intensity non dimensionalized

with inflow bulk velocity U_b were computed and compared with experimental data set of Wang et al.[17,20]

7 Results and discussion

7.1 Qualitative Analysis of flow over BFS and ACDC

Figures 3 and 4 show the instantaneous large coherent structure of ACDC and BFS, respectively using Q criterion. The Q criterion is the second invariant of velocity gradient tensor ∇u and was proposed by Hunt et al.[38] The second invariant $Q = \frac{1}{2}\left(\Omega_{ij}\Omega_{ij} - S_{ij}S_{ij}\right)$. Where $\Omega_{ij} = \frac{1}{2}\left(\frac{\partial u_i}{\partial x_j} - \frac{\partial u_j}{\partial x_i}\right)$ and strain rate tensor $S_{ij} = \frac{1}{2}\left(\frac{\partial u_i}{\partial x_j} + \frac{\partial u_j}{\partial x_i}\right)$ are respectively the anti-symmetric and the symmetric components of ∇u. As it is observed that the boundary layer

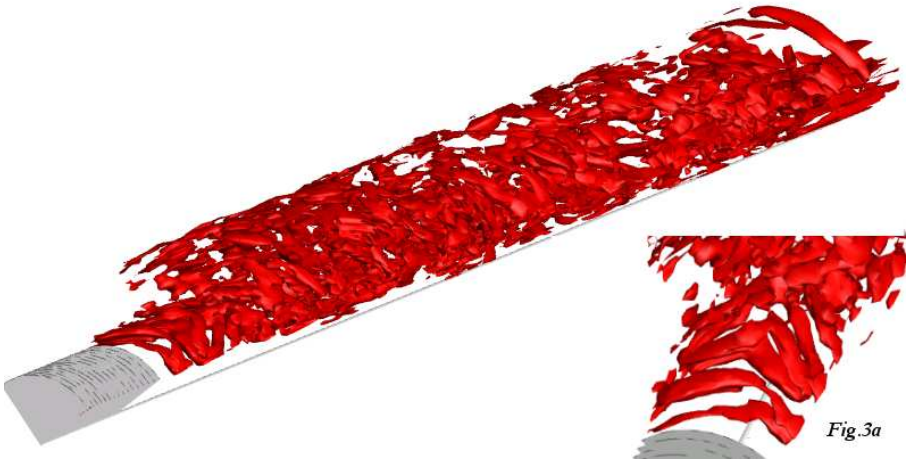

Figure 3: Large Coherent Structure of Axisymmetric Confined Dump Combustor (ACDC) with Q isosurface of 1000

Figure 4: Large Coherent Structure of Backward Facing Step with Q isosurface of 0.5

inside the guiding pipe of ACDC or at the step of BFS, separates at the trailing edge and forms shear layer. The shear layer undergoes the K-H instability and forms the instantaneous coherent structures or eddies of different size. The shear layer attaches downstream at reattachment point and oscillates about the mean reattachment length X_r. The reattachment region is strongly influences with inflow condition, wall and geometry of the configuration. The flow inside the ACDC involve three major flow phenomena as was mentioned by Wang et al.[17,20] a main core, flow between the wall and the shear layer and flow near to the wall.

7.2 Reattachment length of BFS

The mean reattachment length in BFS was X_r= $7.3h$ (Run-4) and $7.1h$ (Run-5) compared to the DNS value of $(X_r = 6.28h)$ of Le et al.[14] and the experimental value of $(X_r = (6.0 \pm 0.15)h)$ of Jovic and Driver.[13] This was because of the inflow boundary condition used in the current simulation did not had turbulent longitudinal vortices's that caused delay in the transition of the shear layer and consequently increase of the reattachment length.[2] Westphal and Johnston[12] observed that the reattachment length decreases with an increase in freestream turbulence. An LES of BFS carried out by Dubief and Delcayre[15] obtained a recirculation length of $7.2h$ at the same Reynolds number of 5100. The inflow boundary condition was mean velocity profile[37] perturbed with white noise.

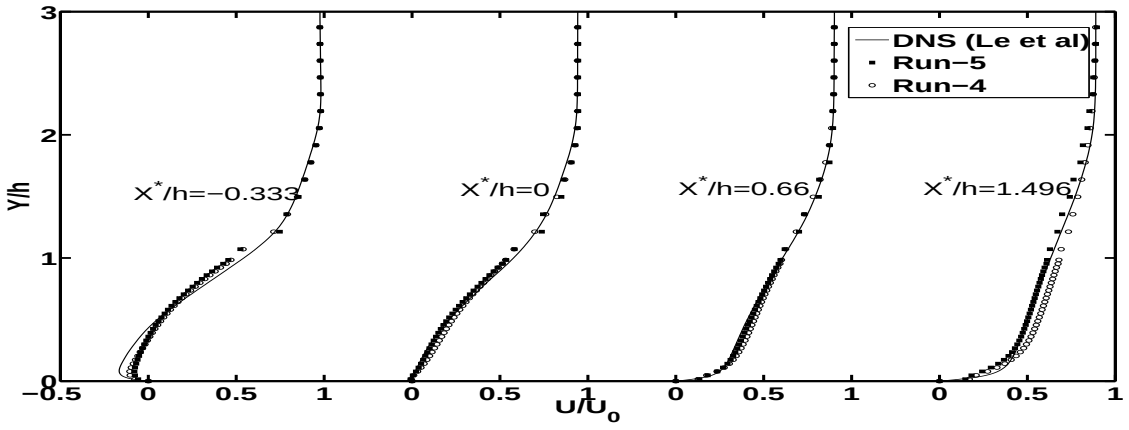

Figure 5: Mean longitudinal velocity profiles at four different streamwise positions downstream of the step, for Run-4 and Run-4 compared to DNS results of Le et al.[14]

7.3 Mean Velocities and Turbulent intensity of BFS

In BFS the averaged flow parameters (velocities etc) are independent of the initial conditions, geometrical parameters and boundary conditions with respect to the normalized coordinate $X^* = x - X_r/X_r$.[12] The non dimensional mean longitudinal velocity profiles were plotted in Fig. 5 at different normalized coordinates X^*. The computed results compared well with the DNS results at the reattachment (X^* = 0) and the recovery region (X^* = 0.66). The longitudinal velocity was under predicated at (X^* =-0.333) especially for $y \leq 0.5h$. The longitudinal velocity was overpredicated at (X^* = 1.497) for Run-4. That is because the coarser grids at this location produced too much diffusion. Less diffusive scheme CDS-4(Run-5) shows improvement over QUICK scheme Fig. 5.

The time-averaged (a) longitudinal $\langle u^{'}u^{'}\rangle^{1/2}/U_0$, (b) vertical $\langle v^{'}v^{'}\rangle^{1/2}/U_0$, (c) spanwise $\langle w^{'}w^{'}\rangle^{1/2}/U_0$ turbulent intensities and (d) Reynolds shear stress component $\langle u^{'}v^{'}\rangle/U_0^2$ are plotted in Fig. 6 at different normalized coordinates X^*. Where $u^{'}$, $v^{'}$ and $w^{'}$ are the velocity fluctuations in longitudinal, vertical and spanwise direction. The longitudinal turbulence intensity compared well with DNS especially for the region $y \leq 1.0h$ and it was underpredicted for the

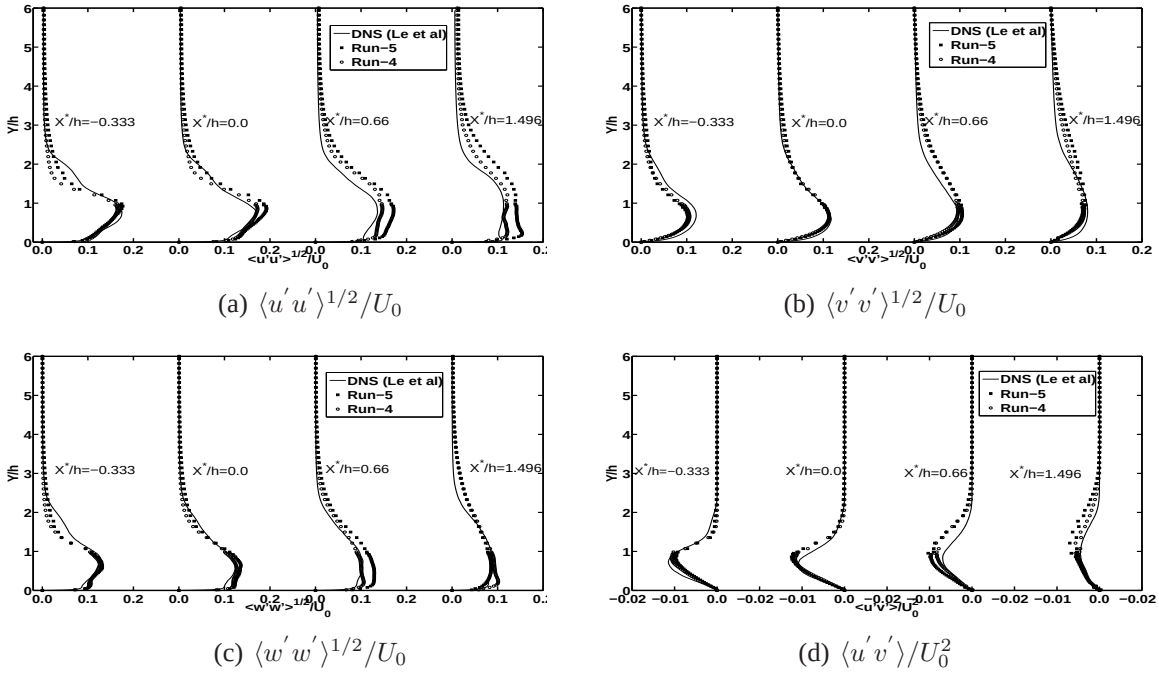

(a) $\langle u^{'}u^{'}\rangle^{1/2}/U_0$ (b) $\langle v^{'}v^{'}\rangle^{1/2}/U_0$

(c) $\langle w^{'}w^{'}\rangle^{1/2}/U_0$ (d) $\langle u^{'}v^{'}\rangle/U_0^2$

Figure 6: Square roots of non-dimensional mean Reynolds stresses at four different streamwise positions downstream of the step for Run-4 and Run-5 compared to DNS results of Le et al.[14]

region $2.2h \geq y \geq 1.0h$ at the reattachment (X^* = 0) and the recirculation (X^* = -0.333). This could be due to two reasons: the first reason was the poor grid resolution for the region $1.0h \leq y \leq 6.0h$, which has reduced the turbulent intensity due to inherent numerical diffusion of QUICK scheme. On the other hand the CDS-4 scheme is less diffusive in nature and predicted more turbulence intensity than the QUICK scheme as shown in Fig. 6. The another reasons was that the inflow boundary condition was not computed as deterministically as it was done in the DNS. The longitudinal turbulent intensity $\langle u^{'}u^{'}\rangle^{1/2}/U_0$ was slightly overpredicted at recovery region (X^* = 0.66, and X^* = 1.497). The vertical turbulent intensity $\langle v^{'}v^{'}\rangle^{1/2}/U_0$ was underpredicted at recirculation(X^* = -0.333) and the prediction is better at the reattachment (X^* = 0). Figure 6d shows the better agreement of Reynolds shear-stress component $\langle u^{'}v^{'}\rangle/U_0^2$ for the region $y \leq 1.0h$.

7.4 Mean Velocities and Turbulent intensity of ACDC

In LES the grid independent solution is essential to understand the influence of subgrid stresses. The present method uses an implicit filter for filtering the governing equations, in that case it is difficult to obtain grid independent LES solution. Because when grids are refined then solution converges towards the DNS. Nevertheless in the present study two grids were studied. Run-1 and Run-2 were the LES of ACDC with grids $(154 \times 88 \times 20)$ and $(154 \times 104 \times 20)$ respectively. The grid is refined in radial direction because the turbulence generation mechanism dominates near the wall and in the shear layer. Figure 7 shows the profiles of the mean and Root Mean Square (RMS) longitudinal velocities for Run-1 and Run-2. It is observed that the mean

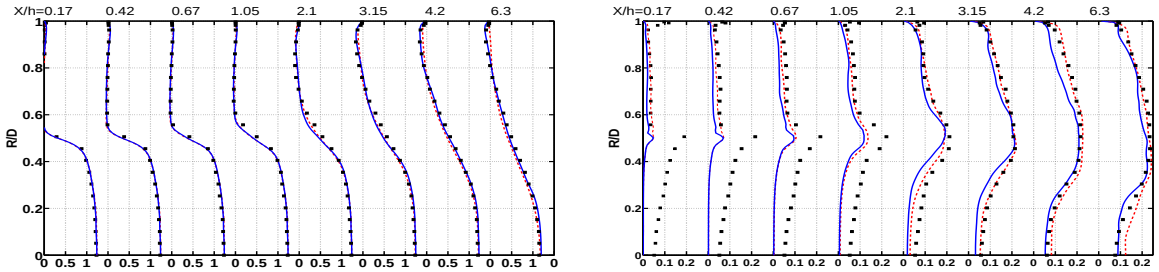

(a) $\left(\frac{U}{U_B}\right)$ (b) $\left(\langle u'u'\rangle^{1/2}/U_B\right)$

Figure 7: Mean and RMS of longitudinal velocity profiles, normalized with bulk velocity U_B, at different streamwise positions downstream of the step; where Run-1 (solid line), Run-2 (dashed line) and experiments (■)

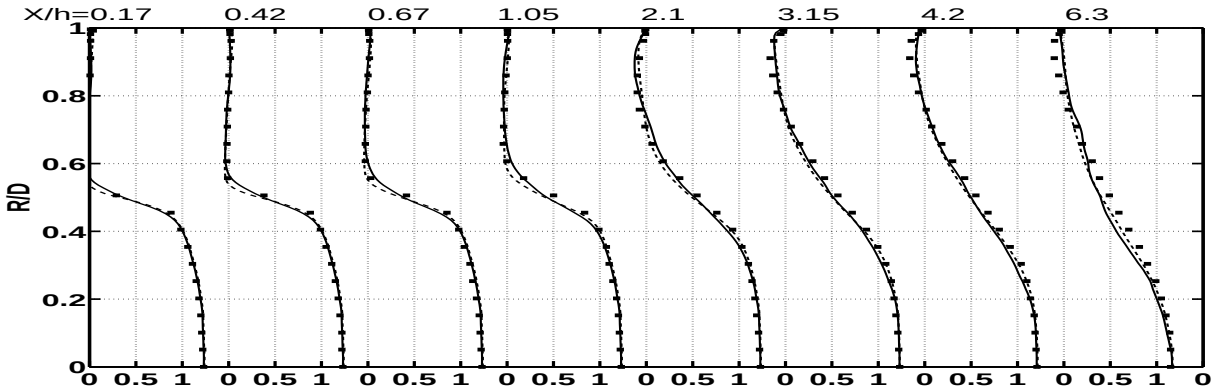

Figure 8: Mean longitudinal velocity profiles, normalized with bulk velocity U_B, $\left(\frac{U}{U_B}\right)$, at different streamwise positions downstream of the step; where Run-2 (dashed line), Run-3 (solid line) and experiments (■)

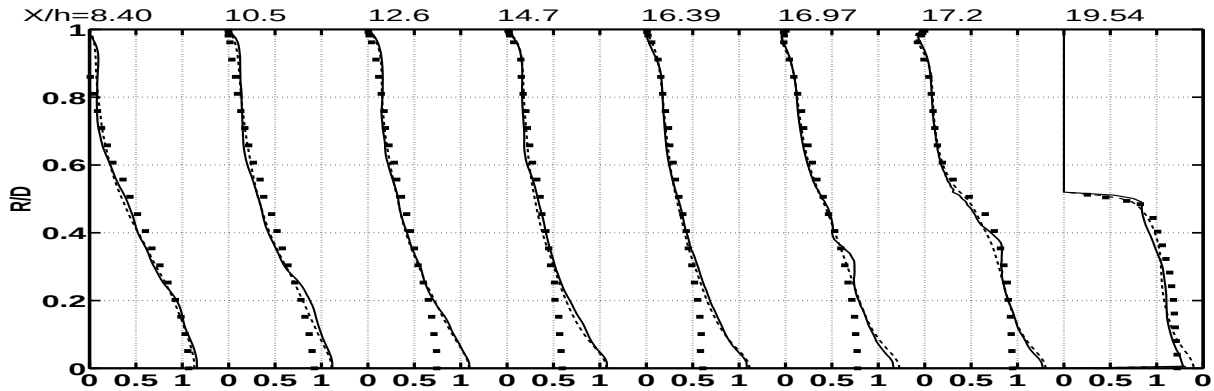

Figure 9: Mean longitudinal velocity profiles, normalized with bulk velocity U_B, $\left(\frac{U}{U_B}\right)$ at different streamwise positions downstream of the step; where Run-2 (dashed line), Run-3 (solid line) and experiments (■)

velocity and RMS do not change much with grid refinement. The RMS values slightly improve close to the reattachment point.

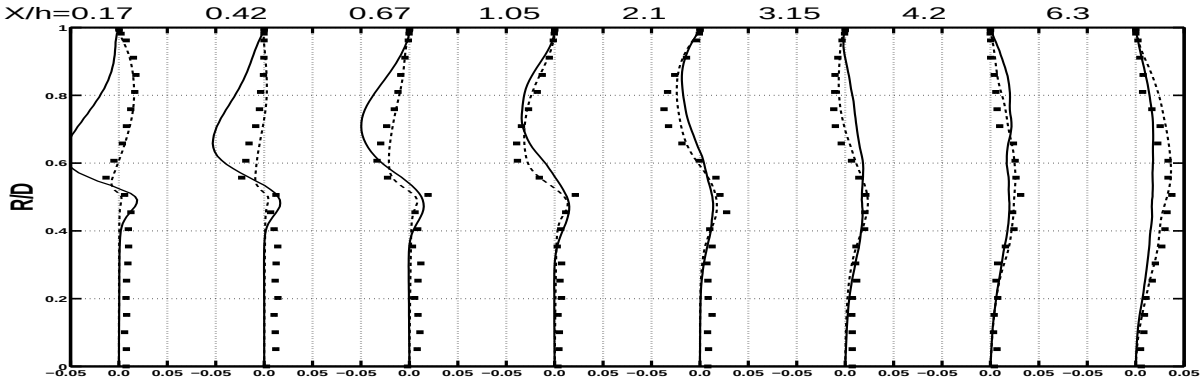

Figure 10: Mean radial velocity profiles, normalized with bulk velocity U_B, $\left(\frac{V_r}{U_B}\right)$ at different streamwise positions downstream of the step; where Run-2 (dashed line), Run-3 (solid line) and experiments (■)

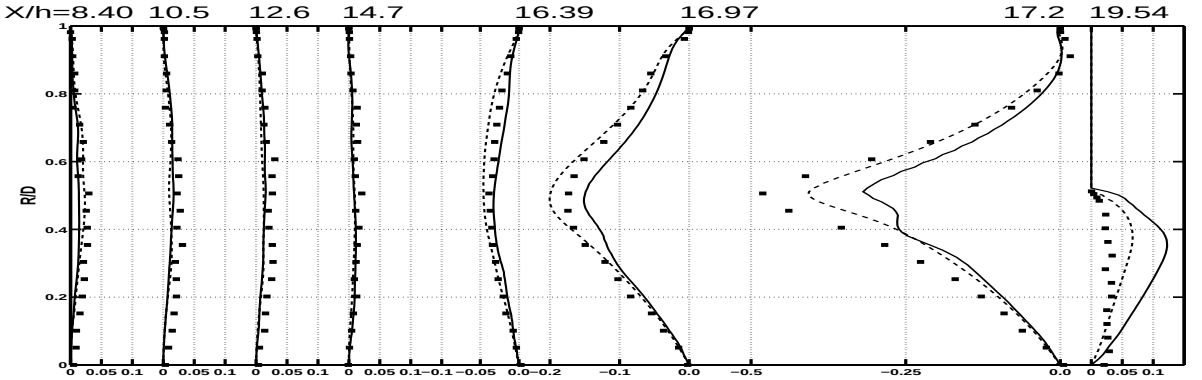

Figure 11: Mean radial velocity profiles, normalized with bulk velocity U_B, $\left(\frac{V_r}{U_B}\right)$ at different streamwise positions downstream of the step; where Run-2 (dashed line), Run-3 (solid line) and experiments (■)

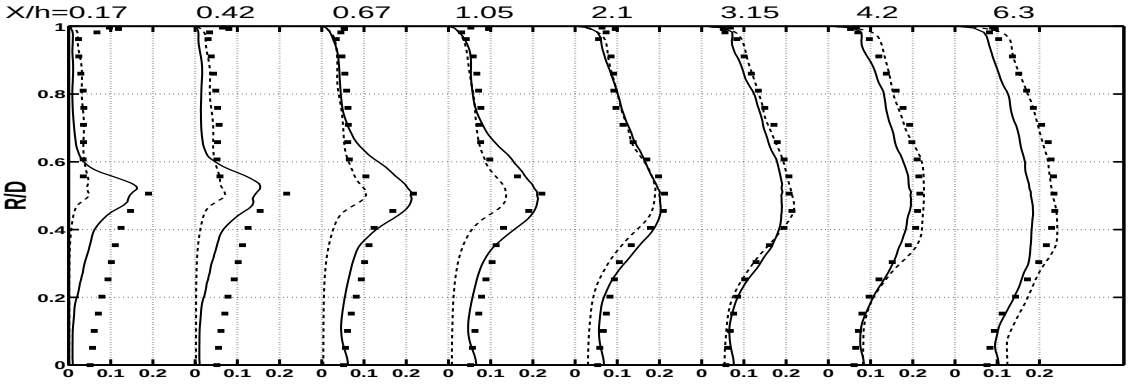

Figure 12: Root Mean Square(RMS) of longitudinal velocity profiles, normalized with bulk velocity U_B, $\left(\langle u^{'}u^{'}\rangle^{1/2}/U_B\right)$, at different streamwise positions downstream of the step; where Run-2 (dashed line), Run-3 (solid line) and experiments (■)

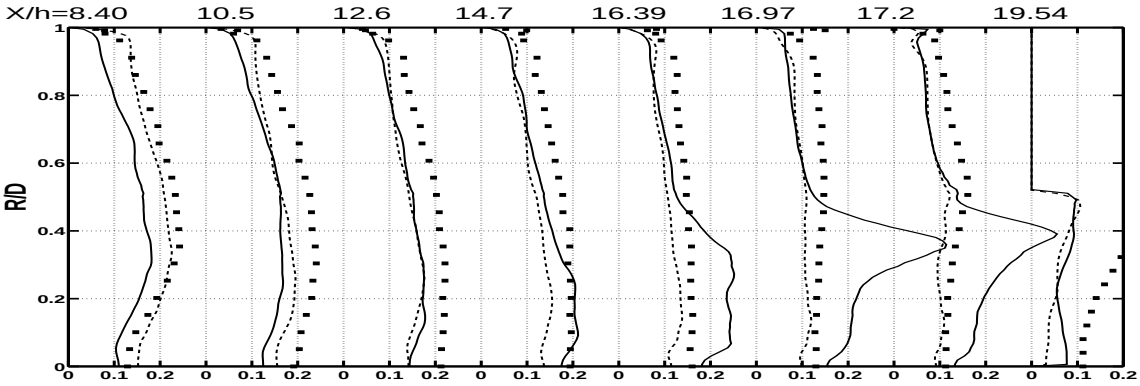

Figure 13: Root Mean Square(RMS) of longitudinal velocity profiles, normalized with bulk velocity U_B, $\left(\langle u^{'}u^{'}\rangle^{1/2}/U_B\right)$, at different streamwise positions downstream of the step; where Run-2 (dashed line), Run-3 (solid line) and experiments (■)

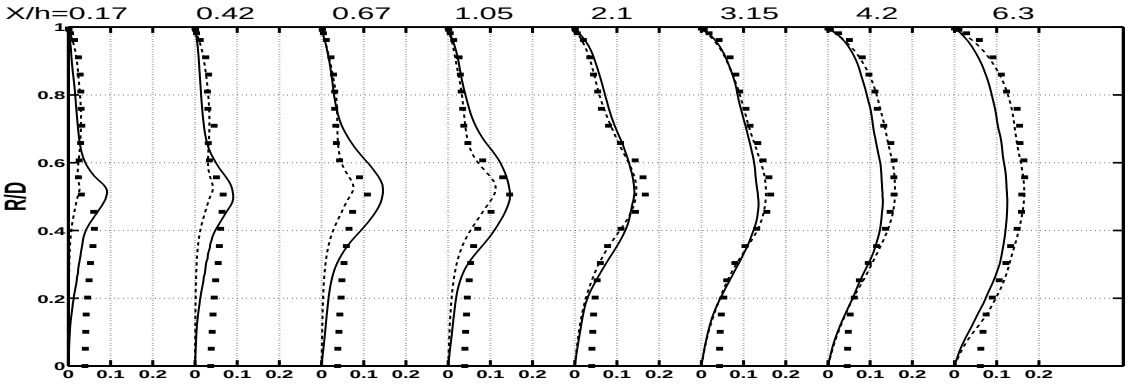

Figure 14: Root Mean Square(RMS) of radial velocity profiles, normalized with bulk velocity U_B, $\left(\langle v_r^{'}v_r^{'}\rangle^{1/2}/U_B\right)$, at different streamwise positions downstream of the step; where Run-2 (dashed line), Run-3 (solid line) and experiments (■)

Figures 8 and 9 show the mean longitudinal velocity normalized with bulk velocity along the axial direction. It can be seen that the reattachment length is well predicated and the secondary recirculation zone which varies from 2.1h to 8.5h is also well predicted. The separation bubble close to constriction is also well captured. It is observed from Figures 8 and 9 that the mean axial velocity matches will with experimental results up to $x/h = 8.4$ and beyond that the core $R/D \leq 0.2$ is overpredicated, where R is the radial coordinates. For $R/D \geq 0.2$ comparison is excellent with experimental data base of Wang et al.[17,20] This overprediction in mean velocities was caused due to the axis boundary condition. As it is seen from Figs.14 and 15 that the radial component of fluctuations are zero at the axis. That clearly indicates that the turbulence was not being redistributed in radial direction, which caused surplus axial momentum and overprediction of mean velocities.

Figures 10 and 11 show the radial velocity profile compared with experiments. The prediction are in good agreement with experiments. The radial component of velocity is very small

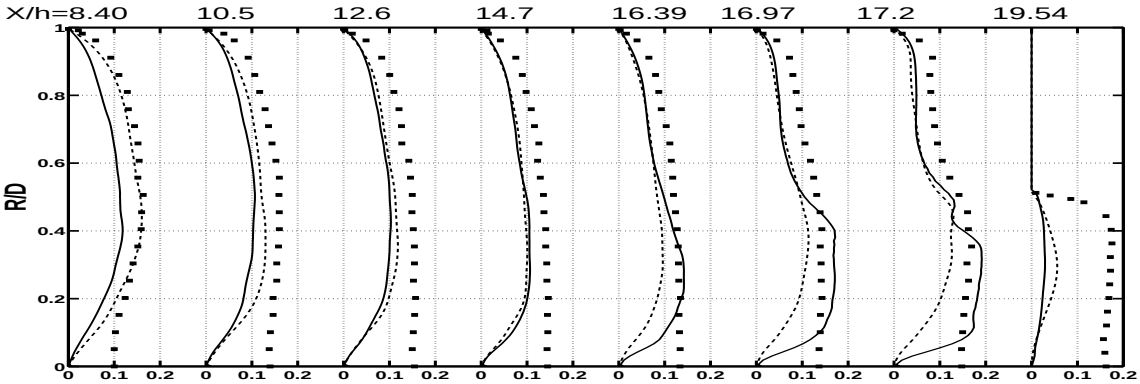

Figure 15: Root Mean Square(RMS) of radial velocity profiles, normalized with bulk velocity U_B, $\left(\langle v_r^{'} v_r^{'} \rangle^{1/2} / U_B\right)$, at different streamwise positions downstream of the step; where Run-2 (dashed line), Run-3 (solid line) and experiments (■)

except in the region $(16 \leq x/h \leq 17.44)$ that is because of the constriction at the exit. Effect of constriction is rather local and the present methodology has captured reasonably well the radial velocity profiles in this region. The turbulence in the region $(2.1 \leq x/h \leq 16)$ is mostly dominate due to K-H instability and subsequent break down of the large coherent structures.

Figures 12 and 13 show the RMS value of the axial velocities. It is observed that the QUICK schemes underpredict the fluctuations close to the sudden expansion. It is because, in current simulation inflow mean profile was subjected with white noise, which did not had properly correlated turbulent length and time scales. These fluctuations dies out due to inherent numerical diffusion of the QUICK scheme. On the other hand CDS-4 scheme predicts better than the QUICK scheme due to low inherent numerical diffusion. Although the fluctuations are underpredicted close to the step but further downstream in the region $(2.1 \leq x/h \leq 8.4)$ the predictions are in good agreement with experiments. This improvement in prediction indicates that the present methodology has captured the turbulence generation process due to shear layer instability and its interaction with wall reasonably well. At the exit the CDS schemes overpredicts the fluctuations due to poor grid resolution in constriction region.

The RMS value of radial velocities as plotted in Figs.14 and 15 are rather large compared to the their mean values Figs.10 and 11. This behavior is quite similar to the BFS where lateral and spanwise variance were much larger than their mean values.[8] That clearly indicate that the flow after sudden expansion is anisotropic.

8 Conclusions

The large eddy simulation approach in curvilinear coordinates is presented. LES in curvilinear coordinates requires two spatial operation, filtering and coordinates transformation. The conventional approach (where filtering is performed prior to coordinates transformation) is preferred rather than the alternate approach (where filtering is performed after the coordinates transformation). Present study showed that the issues raised by Jordan[6] with conventional approach such as calculation of Leonard term and representation of the metric coefficients are not

really the big concern. But instead formulating the dynamic constant with alternate approach created some problems such as non-rotational invariance of the the subgrid viscosity. The remedy to this problem also requires some operations in physical space. The implementation of the dynamic model in alternate approach requires pre and post transformation of the flow variables, which introduces further damping.

Filtering in physical space introduces a commutation error between filtering and differentiation due to non-uniform meshes. The commutation filters up to any desired order have been developed for structured as well as unstructured grids.[27,28] Application of these filters were discussed in curvilinear coordinates. A filter in curvilinear coordinate is developed using the Marsden et al. approach.[27,28] The developed filter is a Laplace filter and is used for explicit filtering the primitive variable. In LES the cost of explicit filtering is hardly 5-6% of total cost.

The present methodology, which is developed in curvilinear coordinates requires computation of orthogonal and non orthogonal terms. For simple geometries computation of non orthogonal terms are not required. Therefore the orthogonal and non-orthogonal terms are treated separately to save the computational time.

The methodology is validated by performing the LES over the backward facing step (BFS) and in the axis symmetric dump combustor (ACDC). The LES over BFS is carried out for a Reynolds number of 5100 based on the inlet free-stream velocity and step height h. The results are validated against DNS data base. The mean longitudinal velocity profile and the turbulence intensities compare satisfactory with the DNS data at the normalized coordinates $X^* = \frac{x-X_r}{X_r}$ for a mesh about 40 times coarser than the DNS. The reattachment length in the longitudinal direction varies from 7.1h to 7.3h as compared to the DNS value of 6.28h, due to inconsistent inflow boundary condition.

The LES of the ACDC is carried out for a Reynolds number of 11700 based on the guiding pipe diameter and the bulk velocity. In order to save computational time, only a 90 degree segment of the geometry is studied. The results are validated against an experimental data base of Wang et al.[17,20] The reattachment length was well predicted and the mean longitudinal, vertical velocity profile and the turbulence intensities compare satisfactory with the experiments.

The influences of the SGS models for practical geometries are less crucial than the discretization and the grid resolution.[8] The overall accuracy depends on the discretization scheme, the grid resolution, inflow and other boundary conditions. The impact of the axisymmetric approach on LES was discussed. The discrepancy in the computed results using axis boundary condition is large at downstream of the step and close to axis. That is because the axis boundary condition does not allow the instantaneous exchange of the mass and momentum across the axis.

ACKNOWLEDGEMENTS

This work has been carried out as a part of Institution-based Strategic Project (ISP) funded by The Research Council of Norway. This support is gratefully acknowledged.

REFERENCES

[1] P. Sagaut. *Large Eddy Simulation for Incompressible flows*. Springer Verlag, 2006.

[2] M. Lesieur, O. Mètais, and P. Comte. *Large-Eddy Simulations of Turbulence*. Cambridge University Press, 2005.

[3] J. H. Ferziger and M. Peric. *Computational Methods for Fluid Dynamics*. Springer Verlag, 2001.

[4] D. G. E. Grigoriadis, J. G. Bartzis, and A. Goulas. Efficient treatment of complex geometries for large eddy simulations of turbulent flows. *Computers & Fluids*, 33(2):201 – 222, 2004.

[5] K. Mahesh, G. Constantinescu, and P. Moin. A numerical method for large-eddy simulation in complex geometries. *Journal of Computational Physics*, 197(1):215 – 240, 2004.

[6] S. A. Jordan. A Large-Eddy Simulation Methodology in Generalized Curvilinear Coordinates. *Journal of Computational Physics*, 148:322–340, January 1999.

[7] V. Armenio and U. Piomelli. A lagrangian mixed subgrid-scale model in generalized coordinates. *Flow, Turbulence and Combustion*, 65:51–81(31), 2000.

[8] B. Panjwani, I. S. Ertesvåg, A. Gruber, and K. E. Rian. Large eddy simulation of backward facing step flow. , 5th National Conference on Computational Mechanics, MekIT09, 2009. Trondheim, Norway.

[9] S. K. Lele. Compact Finite Difference Schemes with Spectral-like Resolution. *Journal of Computational Physics*, 103:16–26, November 1992.

[10] W. W. Kim and S. Menon. An unsteady incompressible Navier-Stokes solver for large eddy simulation of turbulent flows. *International Journal for Numerical Methods in Fluids*, 31:983–1017, November 1999.

[11] J. K. Eaton and J. P. Johnston. A review of research on subsonic turbulent flow reattachment. *AIAA Journal*, 19:1093–1100, September 1981.

[12] R. V. Westphal and J. P. Johnston. Effect of initial conditions on turbulent reattachment downstream ofa backward-facing step. *AIAA Journal*, 22:1727–1732, December 1984.

[13] S. Jovic and D. M. Driver. Backward-facing step measurements at low Reynolds number, Re=5000. *NASA Technical Memorandum NO:108807*, pages 1–24, February 1994.

[14] H. Le, P. Moin, and J. Kim. Direct numerical simulation of turbulent flow over a backward-facing step. *Journal of Fluid Mechanics*, 330:349–374, January 1997.

[15] Y. Dubief and F. Delcayre. On coherent-vortex identification in turbulence. *Journal of Turbulence*, 1:1–22, December 2000.

[16] E. C. Fernandes, M. V. Heitor, and S. I. Shtork. An analysis of unsteady highly turbulent swirling flow in a model vortex combustor. *Experiments in Fluids*, 40(2):177–187, Feb 2006.

[17] P. WANG and X. S. BAI. Large eddy simulations of turbulent swirling flows in a dump combustor: a sensitivity study. 47(2):22, 2005.

[18] A. Afshari, F. A. Jaberi, and T. I.-P. Shih. Large-Eddy Simulations of Turbulent Flows in an Axisymmetric Dump Combustor. *AIAA Journal*, 46:1576–1592, July 2008.

[19] O. Lucca-Negro and T. O'Doherty. Vortex breakdown: a review. *Progress in Energy and Combustion Science*, 27(4):431 – 481, 2001.

[20] P. Wang, X. S. Bai, M. Wessman, and J. Klingmann. Large eddy simulation and experimental studies of a confined turbulent swirling flow. *Physics of Fluids*, 16(9):3306–3324, 2004.

[21] J. U. Schlüter. Influence of axisymmetric assumptions on large eddy simulations of a confined jet and a swirl flow. *International Journal of Computational Fluid Dynamics*, 18(3):235–245, 2004.

[22] M. Vinokur. An analysis of finite-difference and finite-volume formulations of conservation laws. *Journal of Computational Physics*, 81(1):1–52, 1989.

[23] M. Vinokur. On One-Dimensional Stretching Functions for Finite Difference Calculations. *Journal of Computational Physics*, 50, May 1983.

[24] S. A. Jordan and A Ragabs. A large-eddy simulation of the near wake of a circular cylinder. *American Society of Mechanical Engineers*, 120(2), 1998.

[25] S. Ghosal and P. Moin. The basic equations for the large eddy simulation of turbulent flows in complex geometry. *J. Comput. Phys.*, 118(1):24–37, 1995.

[26] H. van der Ven. A family of large eddy simulation (LES) filters with nonuniform filter widths. *Physics of Fluids*, 7:1171–1172, May 1995.

[27] O. V. Vasilyev, T. S. Lund, and P. Moin. A general class of commutative filters for les in complex geometries. *J. Comput. Phys.*, 146(1):82–104, 1998.

[28] A. L. Marsden, O. V. Vasilyev, and P. Moin. Construction of commutative filters for les on unstructured meshes. *Journal of Computational Physics*, 175(2):584 – 603, 2002.

[29] B. J. Geurts and D. D. Holm. Commutator errors in large-eddy simulation. *Journal of Physics A: Mathematical and General*, 39(9):2213, 2006.

[30] F. Bahramian and A. G. Straatman. A volume-based discrete test filter for conducting large eddy simulations with application to physiological flow in a constricted tube. *International Journal for Numerical Methods in Fluids*, 2009.

[31] M. Germano, U. Piomelli, P. Moin, and W. H. Cabot. A dynamic subgrid-scale eddy viscosity model. *Physics of Fluids A: Fluid Dynamics*, 3(7):1760–1765, 1991.

[32] C. M. Rhie and W. L. Chow. Numerical study of the turbulent flow past an airfoil with trailing edge separation. *AIAA Journal*, 21:1525–1532, November 1983.

[33] A. J. Chorin and J. E. Marsden. *A Mathematical Introduction to Fluid Mechanics*. 3rd ed. Springer Verlag, 1993.

[34] M. H. Carpenter and C. A. Kennedy. Fourth-order 2N-storage runge-kutta schemes. NASA Technical Memorandum NASA -TM 109112, pages 1-26, June 1994.

[35] M. Mizukami, N. J. Georgiadis, and M. R. Cannon. A comparative study of computational solutions to flow over a backward-facing step. In *its The Fifth Annual Thermal and Fluids Analysis Workshop p 523-530 (SEE N94-23634 06-34)*, pages 523–530, November 1993.

[36] D. M. Kuehn. Effects of Adverse Pressure Gradient on the Incompressible Reattaching Flow over a Rearward-Facing Step. *AIAA Journal*, 18:343–344, March 1980.

[37] P. R. Spalart. Direct simulation of a turbulent boundary layer up to **Re** 1410. *Journal of Fluid Mechanics Digital Archive*, 187:61–98, 1988.

[38] J.C.R. Hunt, C.A.A. Wray, and P. Moin. Eddies, streams, and convergence zones in turbulent flows. Technical report, Center for Turbulence Research Report CTR-S88, Stanford University, 1988.